IOP Publishing Nanotechnology
Nanotechnology 29 (2018) 335304 (11pp) https://doi.org/10.1088/1361-6528/aac84a

Nanoink bridge-induced capillary pen printing for chemical sensors

Seong-Joong Kahng[1], Chiew Cerwyn[1], Brian M Dincau[2], Jong-Hoon Kim[2], Igor V Novosselov[1], M P Anantram[3] and Jae-Hyun Chung[1]

[1] Department of Mechanical Engineering, University of Washington, Seattle, WA 98195, United States of America
[2] Department of Mechanical Engineering, School of Engineering and Computer Science, Washington State University, Vancouver, WA 98686, United States of America
[3] Department of Electrical Engineering, University of Washington, Seattle, WA 98195, United States of America

E-mail: jae71@uw.edu

Received 19 February 2018, revised 24 April 2018
Accepted for publication 29 May 2018
Published 13 June 2018

Abstract

Single-walled carbon nanotubes (SWCNTs) are used as a key component for chemical sensors. For miniature scale design, a continuous printing method is preferred for electrical conductance without damaging the substrate. In this paper, a non-contact capillary pen printing method is presented by the formation of a nanoink bridge between the nib of a capillary pen and a polyethylene terephthalate film. A critical parameter for stable printing is the advancing contact angle at the bridge meniscus, which is a function of substrate temperature and printing speed. The printed pattern including dots, lines, and films of SWCNTs are characterized by morphology, optical transparency, and electrical properties. Gas and pH sensors fabricated using the non-contact printing method are demonstrated as applications.

Supplementary material for this article is available online

Keywords: single-walled carbon nanotubes, capillary pen, pH sensor, gas sensor, printing

(Some figures may appear in colour only in the online journal)

1. Introduction

Since the discovery of carbon nanotubes (CNTs), various patterning methods have been investigated to develop chemical and biological sensors. Early methods relied on direct growth on a substrate, assembly using an electric field, and self-assembly [1–3]. In the fabrication of wearable sensors, a non-contact printing is preferred to avoid potential damage to the substrate or existing layers. Thermal and piezoelectric inkjet printing methods [4–6] rely on thermal expansion or electromechanical vibration to eject droplets [5, 7]. Due to the droplet formation physics, inkjet printing is challenging for nanoink of low viscosity and high surface tension [8, 9] which often requires significant modifications of ink properties [10–12]. To achieve electrical conductance of the printed CNT patterns, the discrete nature of droplet deposition requires the ejector shift to connect the drops. In the printing of biological materials, the fragile biomolecules may not be compatible with the high pressures, heat, and shear stresses associated with inkjet printing [9, 13, 14]. Electrohydrodynamic printing utilizes an electric field to control flow through a nozzle [15–17], but it is limited to a conductive and semi-conductive substrate. Stencil printing [18] deposits nanomaterial by spraying through a mask, which is limited to the designed masking pattern.

As an alternative, fountain pens [19–21], ball pens [22], and pencils [23, 24] have been demonstrated to draw nanomaterials. For fountain pens, the capillary force attracts ink into the tube and provides the pressure gradient to hold ink column inside. When the capillary tube is in contact with porous paper, the capillary pressure in a pen decreases due to the contact between the nib and the porous substrate, resulting in ink flow [25]. However, printing on an impermeable film is more challenging as the contact angle is much greater than 0°.

 © 2018 IOP Publishing Ltd Printed in the UK

Moreover, any contact printing may damage the substrate [20] hindering multiple layer deposition required for complex sensor structures.

In this paper, a non-contact capillary pen printing method is presented. The technique is demonstrated by patterning single-walled carbon nanotubes (SWCNTs) via a nanoink liquid bridge. The non-contact printing method does not physically damage the substrate or previously deposited layers. A single pass printing is sufficient to obtain a measurable electrical resistance. The resistance and the optical properties are characterized for several print geometries: a dot, a line, and a film. The use of the printing method for fabrication of CNT based gas sensors and pH sensor is explored as a potential application.

2. Nanoink bridge-induced printing

The non-contact capillary method deposits nanoink through a liquid bridge forming between a capillary pen and substrate (figure 1(a)). A stylographic pen consists of a capillary nozzle and a rod-shaped ink stopper that assures nanoink seal when the pen is not used. During printing, two geometric parameters require control in order to maintain the capillary bridge integrity: the pen tip height (H) from the substrate and the advancing bridge contact angle (θ_{B_a}) as illustrated in figure 1(a). When the liquid bridge is established, the ink flow rate depends on the pressure difference between the capillary pen reservoir and the substrate surface. In a static condition, θ_{B_a} is dependent on the substrate surface properties, its temperature, and ink properties. When the pen moves to the right, θ_{B_a} increases, and the recessing angle (θ_{B_r}) decreases. As θ_{B_a} increases, the hydrostatic pressure on surface increases to reduce the ink flow. For low θ_{B_a}, the pressure difference is maximized resulting in the high ink feed rate.

Figure 1(b) shows the printing setup consisting of an x–y–z plotter and control module. The printing direction is controlled by two step motors in x and y directions. Manual micropositioning stage sets the Z-coordinate (pen tip height; H) necessary to form a nanoink bridge. A camera with a microscopic objective lens monitors the condition of the liquid bridge for a feedback control. The substrate temperature is controlled via closed-loop by a thermocouple as a sensor for a heating stage.

Figure 1(c) illustrates the printing procedure. First, the nib is pressed in the axial direction, and nanoink is released due to capillary action. Second, upon the release of the nanoink, the pen is withdrawn from the substrate to $H = 100\ \mu$m; nanoink bridge forms between the pen tip and the substrate. When the pen moves to the right, θ_{B_a} increases and θ_{B_r} decreased. Finally, the pen is retracted to stop the print. Figure 1(d) shows a typical example of the printed pattern using the nanoink bridge printing on a polyethylene terephthalate (PET) film. A PET film is an appropriate substrate for chemical sensors because it is chemically resistant, transparent and mechanically robust.

3. Experimental methods

3.1. Characterization of printing method

To study the printing characteristics, a dot, a line and a film of SWCNTs were printed at various substrate temperatures and printing speeds. Temperature and printing speeds were controlled to obtain uniform line width and consistent electrical resistance because contact angle, viscosity and evaporation effect were critical factors to determine the printing quality. Nanoink was prepared by suspending SWCNTs (5 mg ml^{-1}) in 1% sodium dodecyl sulfate (SDS) by sonication. In the suspension, the supernatant was used as nanoink. The advancing contact angle (θ_{B_a}) on a PET film was measured for various substrate temperatures and printing speeds. The morphology of the printed patterns and the electrical properties were characterized. The nominal diameters of the capillary pens were 100, 300, and 700 μm. The outer diameters of the pen nib (D_o in figure 1(a)) were 225, 375, and 790 μm, respectively (supplementary information; figure S1 is available online at stacks.iop.org/NANO/29/335304/mmedia). The outer diameters determined the minimum line width in printing as the meniscus attached to the outer dimension of the nib. In the paper, the nominal diameters are used hereafter. The printer was located in a laminar flow hood. The temperature and the relative humidity in the chamber were 26 ± 1.0 °C and 35 ± 2.0%, respectively.

3.1.1. Dot printing. A single dot was printed at various substrate temperatures 20 °C, 40 °C, 60 °C, 80 °C, and 100 °C using a 300 μm diameter pen. The pen reservoir was filled with SWCNT-ink and then installed on a printer. The pen was pressed and then withdrawn to $H = 100\ \mu$m to form a nanoink bridge. To study the evaporation characteristics, the holding time was controlled at 1, 5, and 10 s at each temperature. The contact angles (θ_B) were measured for each case by using the camera images in the printer. The height profile of the dots was scanned by a profilometer (Alpha-step D-300 stylus profiler, KLA-Tencor Corporation).

3.1.2. Line printing. To print a line, numerical control (G-code) was used to control x and y directional step motors. A 100 μm capillary pen was used. After the nanoink bridge formed at a 100 μm gap, a straight line was deposited on a PET film. Printing speed was set in the range from 0.2 to 10 mm s^{-1}, and the temperature was controlled from 20 °C to 100 °C. The line width and θ_{B_a} were measured for each speed and temperature. After printing, a silver paste was applied to both ends of the line to form electrodes. A picoammeter (6487 Picoammeter/Voltage Source, Keithley Instruments) was used to measure current–voltage (I–V) characteristics of the printed line. The printed line was imaged by an optical microscope (Olympus BX-41, Olympus, Gaithersburg, MD, USA) and scanning electron microscopy

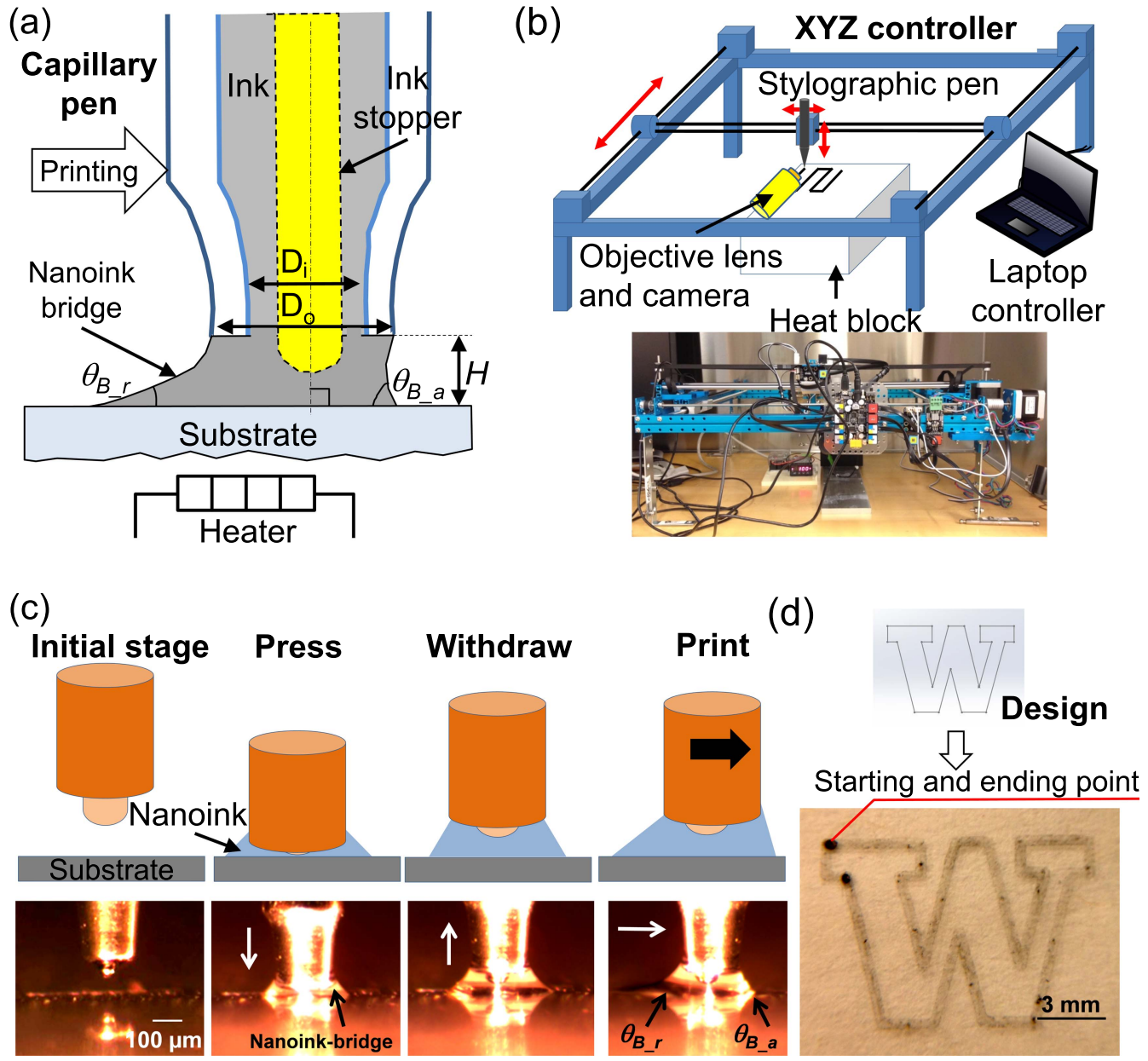


Figure 1. Nanoink bridge-induced capillary printing (a) printing concept (b) schematic of an XYZ plotter installed with a heating stage and a camera system. The top image shows a printing system, and the bottom is a photograph of the setup. (c) Nanoink bridge-induced printing using water ink on a PET film. The ink is released by pressing the stopper. Upon withdrawal by 100 μm, an ink bridge forms. The advancing contact angle increases as the pen moves from left to right. (d) W-pattern printed by SWCNT-ink at 80 °C at 1.2 mm s^{-1}. The top image shows a design.

(SEM) in order to characterize the morphology of SWCNT lines.

3.1.3. Film printing. Film printing was achieved by drawing continuous lines in a linear hatch pattern covering the area of 15 × 15 mm^2. The printing speed was set for 2.5 mm s^{-1}, and the substrate temperature was varied from 20 °C to 100 °C. The nominal diameter of a capillary pen was 700 μm. To achieve complete coverage, the pen was shifted by 600 μm for each pass (total of 25 parallel passes). Optical transparency measurements were performed by transmission optical microscopy (Olympus BX-41, Olympus, Gaithersburg, MD, USA). The transparency was computed as a ratio of the transmitted white light intensity through the printed area over the non-printed area. The sheet resistance was measured using a custom 4-point probe measurement system (supplementary information; figure S2).

3.2. Doping effect

The electrical characteristics of the SWCNT lines were studied for doping polyethyleneimine (1% PEI, Fluka). The printing sequence was varied for PEI and SWCNTs. In one case, SWCNT lines were printed first, followed by PEI deposition (SWCNT/PEI). In the other case, the order was reversed. The SWCNT lines were printed on top of PEI (PEI/SWCNT).

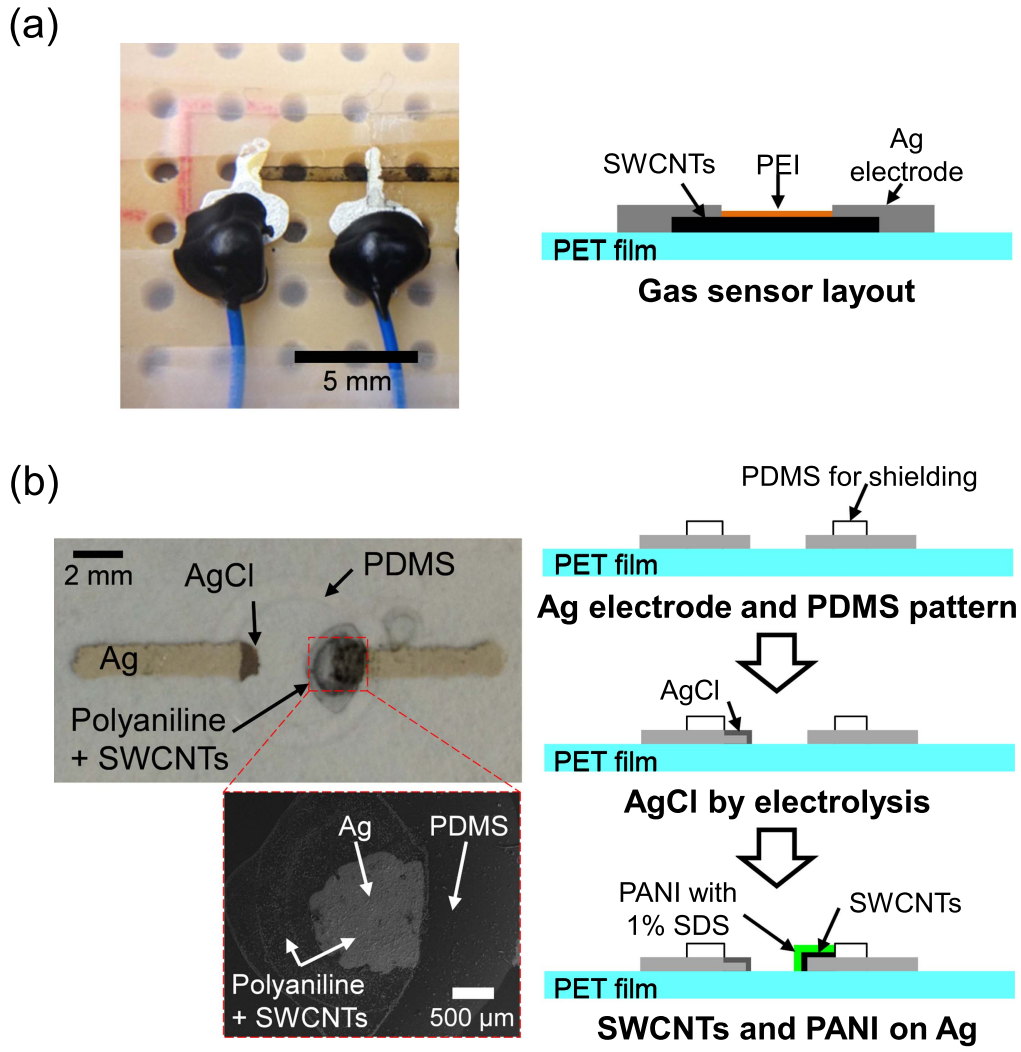


Figure 2. Fabrication steps (a) images and cross-section of a SWCNT-gas sensor (b) optical and SEM images and fabrication steps of a SWCNT-pH sensor.

The printing conditions were 80 °C with printing speed of 0.83 mm s^{-1} where a stable line pattering could be obtained. Silver electrodes were patterned on the SWCNT lines. For both cases of SWCNT/PEI and PEI/SWCNT depositions, PEI solution (1 μl) was dispensed by 1, 2, and 3 times in order to analyze a doping effect and electrical stability. After each deposition, PEI was cured in a convection oven at 100 °C for 1 h. *I–V* characteristics were measured for all cases.

3.3. Sensor fabrication

3.3.1. Gas sensor. To fabricate a gas sensor, SWCNT electrode was printed as a line using a 300 μm diameter pen (figure 2(a)). The substrate temperature was held at 80 °C, and printing speed was 0.83 mm s^{-1}. Silver ink was deposited on both ends of the SWCNTs for electrical connection. The SWCNT electrode was functionalized by depositing 1 μl drop of 1% PEI, which was cured for 1 h at 100 °C in a convection oven. A second SWCNT electrode was coated with 1 μl drop of 1% Nafion (Nafion 117 solution, Sigma-Aldrich Co, LLC.) and cured for 1 h at 120 °C in a convection oven. Both sensors were exposed to two different concentrations of NO_2 (8 and 22 ppm). The sensors' resistance was measured and recorded by a multimeter (287 True RMS Multimeter, Fluke Corporation).

3.3.2. pH sensor. Silver electrodes were screen-printed on PET film (figure 2(b)), which was cured at 100 °C for 10 min (supplementary information; figure S3). Polydimethylsiloxane (PDMS; Sylgard 184 silicone elastomer, Dow Corning Corporation) was stamped in a ring shape to hold analyte solution inside the ring. The PDMS was cured at 75 °C for 1 h in a convection oven. One of the silver electrodes (cathode) was modified to form an AgCl layer by electrolysis (1.5 Vdc for 1 min in 1 M HCl solution). For the other electrode (anode), SWCNT lines were printed on silver electrodes with speed of 0.83 mm s^{-1} using a 300 μm diameter pen that covered the entire silver electrode surface. The printing temperature was 80 °C. The printing was performed like film printing to cover the square area of 1 mm^2. The printing conditions were 80 °C. The SWCNT printed electrode was cured for 10 min on a 100 °C hotplate. Polyaniline (5 mg ml^{-1}; PANI; emeraldine

salt, Sigma-Aldrich Co, LLC.) suspended in 1% SDS was deposited on top of the SWCNT electrode using two 1 μl drops, followed by curing at 120 °C for 1 h. The voltage between the AgCl electrode and PANI electrode was measured using an Arduino circuit for standard pH solutions of pH 4, 7, and 10 (Omega Engineering, Inc.). Since the circuit measured the voltage difference ranging 0–3 V, a 1.61 V AA battery was serially connected to shift the voltage potential above 0 V in the control pH ranges (pH 7–10).

4. Results and discussion

4.1. Characterization of printing method

4.1.1. Dot printing. The section aims to characterize dot printed patterns at various temperatures and holding times. In the results, 60 °C showed the dot diameter to the nib diameter ratio of 1 with the uniform distribution of the SWCNTs due to a reduced coffee ring effect.

A circular dot printed pattern formed when a capillary pen was pressed and retracted to 100 μm on a PET film for 1, 5, and 10 s (figure 3(a)). As the temperature increased, the ratio of the dot diameter to the outer nib diameter decreased and approached unity (figure 3(b)). The dot size reduction was attributed to the increase of the static contact angle (θ_{B_a}) and the pinning at the meniscus due to ink evaporation on the hot surface. As the substrate temperature increased, the surface tension and the viscosity decreased, however, the evaporation rate increased θ_{B_a} (figure 3(c)). As θ_{B_a} approached 90°, the meniscus edge was pinned yielding the ratio of unity. As the substrate temperature increased, the drop spreading on the substrate was reduced suggesting the effects of the increased evaporation rate at the drop edge. When the pen was withdrawn from the substrate, evaporation times decreased from 33 to 1 s as the temperature increased from 20 °C to 100 °C (supplementary information; figure S4).

Profilometer measurements of the dot depositions show that a coffee ring effect is present for a higher substrate temperature (figure 3(d)). The greatest deposition height occurred for prints with the surface temperature of 100 °C. During the deposition, SWCNTs were continuously delivered to the edge of the ink bridge where the liquid evaporation rate was the greatest, resulting in an increased local concentration of the SWCNTs in the solution, thus their thickest deposition at the dot edges. At room temperature, relatively uniform distribution of SWCNT-ink was observed as the ink flow rate, and its deposition rate was balanced by the evaporation rate.

4.1.2. Line printing. The section aims to characterize printed lines at various temperatures and printing speeds. In the results, 60 °C and 80 °C showed uniform line width under the printing speed of 2.5 mm s^{-1} with a reduced coffee ring effect.

Microscopic observation of the printed line patterns shows that three distinct printing regions exist: (region 1) print line width decreases with the increase of print speed in the low-temperature prints (20 °C and 40 °C); (region 2) line width is constant at medium temperature (60 °C and 80 °C); (region 3) line width increases with print speed—at high temperature (100 °C) and lower speeds. The trend is due to changing fluid properties and θ_{B_a}.

Region 1 was observed at the lower temperature conditions (20 °C and 40 °C) and medium temperature (60 °C) at higher print speeds; the line width reduced with the increase in print speed and the increase of the substrate temperature (figures 4(a) and (b)). At room temperature, the normalized line width, which is the ratio of the printed line width to the actual outside diameter of a Rotring pen, was reduced from 2.5 to 1 as the print speed increased from 0.2 to 2.5 mm s^{-1}. The nominal and actual diameters are given in the supplementary information (figure S1). At the low print speed, low contact angle and low shear stress, the line width was not uniform, indicating the unstable behavior of the capillary bridge. As the print speed increased both shear stress and contact angle, the bridge was stabilized, resulting in the stable printing conditions exhibiting constant line width and lower flow rate, which was also consistent with the increased sheet resistance. The reduction of the line width suggests that (i) the increased θ_{B_a} (figure 4(c)) causes the increase in the contact angle on the sides of the droplet parallel to the nib motion due to the surface tension, (ii) capillary bridge elongated along the printing direction with the shear stress. For the lower temperature condition, the prints failed at the speeds >2.5 mm s^{-1}, as θ_{B_a} approaches 90°.

Region 2 was characterized by relatively constant line width independent of the print speed at 60 °C and 80 °C. At the higher temperatures, the ink viscosity reduced resulting in the lower local shear stress allowing the ink to flow more uniformly at the larger contact angle. Experimentally the print speed increasing from 2.5 mm s^{-1} to 10 mm s^{-1} did not compromise the bridge stability though the advancing angle exceeded 90° for the faster prints. The high θ_{B_a} resulted in the high and stable contact angles on both sides of the bridge.

Region 3 was characterized by the increase in the line width as print speed increased at $T = 100$ °C and print speed below 2.5 mm s^{-1}. It is speculated that the effect was caused by the high rate of ink evaporation at the low print speeds as the liquid in the bridge approached its boiling point. As the speed increased, the time allowed for evaporation reduced. The ink was delivered to the substrate more effectively resulting in wider print line. At the higher speeds (>2.5 mm s^{-1}), the normalized line width reduced, which was consistent with the increase of θ_{B_a} as shown in figure 4(c).

Related to the optimization of the print conditions: at the temperatures greater than 60 °C, SWCNTs could be printed as $\theta_{B_a} > 90°$. At the temperature of 80 °C and 100 °C, a stick-slip effect was observed at the advancing meniscus of a nanoink bridge. The beach mark pattern in figure 4(a) and an SEM study were consistent with the stick-slip effect (supplementary information; figure S5). Similar to the dot printing, the printed lines showed a coffee ring effect at the temperature >60 °C while a flat profile was observed at the temperature <60 °C. The thickness of the printed line was

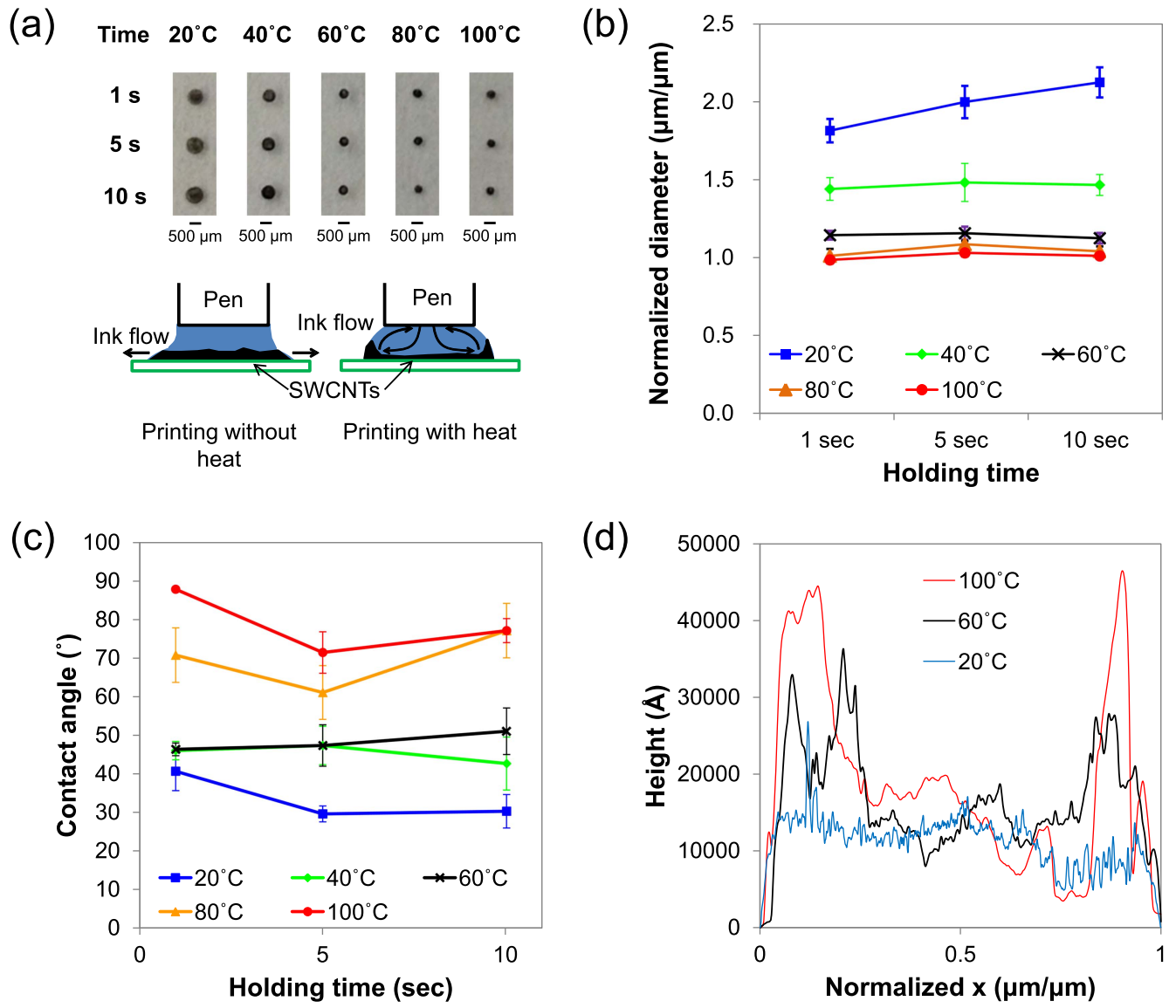


Figure 3. Dot printing (a) dots printed at surface temperature 20 °C–100 °C with holding time of 1, 5, and 10 s. Scale bar: 500 μm (b) dot diameters normalized by an outer nib diameter (c) contact angles according to holding time (d) dot profile at 20 °C, 60 °C, and 100 °C (1 s holding time).

well below 1 μm, which could not be measured by a profilometer or an atomic force microscope because of the relatively rough PET surface. The formation of the coffee ring could be observed by the higher contrast in an optical microscope and SEM (supplementary information; figure S4).

For electrical characterization of the prints, a silver electrode was patterned at the ends of a printed line. In comparison to 4-point probe measurement, the contact resistance using the 2-silver electrodes was only 9.6 ± 0.6%, which was consistent throughout multiple measurements ($N = 6$). The *I–V* characteristics showed a linear trend due to the metallic SWCNTs in the printed lines. The sheet resistance of the lines became larger as both temperature and speed became higher (figure 4(d)). With the increase of θ_{B_a}, the smaller pressure difference reduced the flow rate of SWCNT-ink, which increased the sheet resistance.

Overall, the increase in the print speed yielded the greater sheet resistance as a result of higher contact angle and reduced flow rate. At the higher speed, the contact angle increased the pressure on the substrate, which resulted in the smaller nanoink flow rate thus the reduction of SWCNTs deposition and greater transparency of the print (supplementary information, figure S6). Unlike in the inkjet printing, both desired transparency and electrical resistance could be obtained with single print, which shows the advantage of the nanoink bridge-induced capillary printing.

4.1.3. Film printing. The section aims to characterize two-dimensional printing at various temperatures. In the results, 60 °C showed relatively high optical transmission and low sheet resistance.

For film printing, the area of 15 × 15 mm^2 was printed in 3 min with the nib speed of 2.5 mm s^{-1} (supplementary

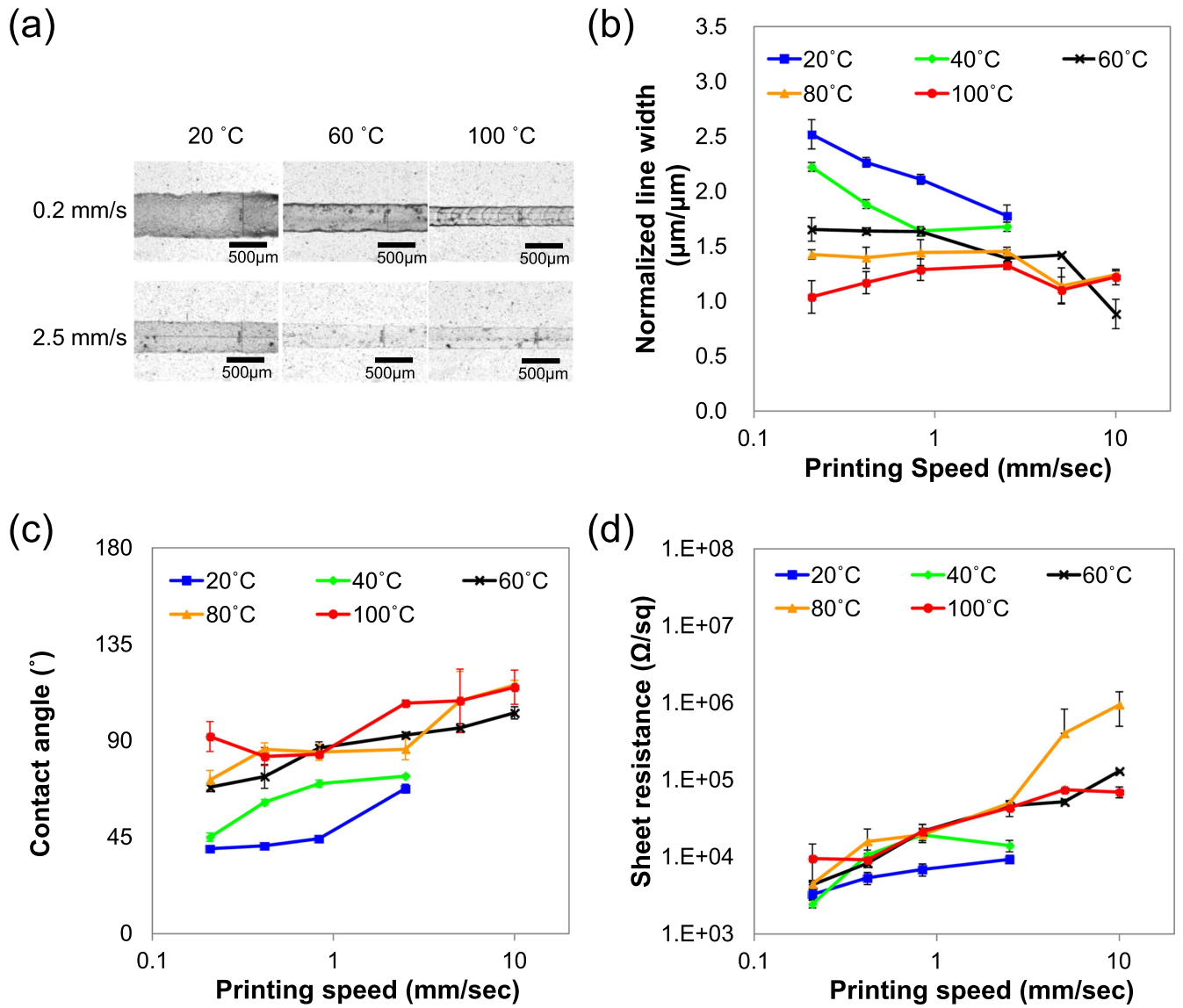


Figure 4. Line printing (a) printed lines at 0.2 and 2.5 mm s^{-1} under the substrate temperature of 20 °C–100 °C. (b) Normalized line widths at a temperature of 20 °C–100 °C with a printing speed of 0.2–10 mm. (c) Advancing contact angle ($\theta_{B,a}$) at various printing speeds. (d) Sheet resistance according to print temperature and speed.

material; movie file). When the printing lines were overlapped at $T = 20$ °C, the nanoink was smudged across the printed lines. The optical transparency of the film increased from 67% to 89% as the temperature increased (figure 5(a) and supplementary information; figure S7). For print temperatures >60 °C, SWCNT clusters were observed; during printing, the SWCNTs were aggregated at the stopper, leaving clusters on the substrate. The sheet resistance increased from 2.5 to 62.4 kΩ/sq as the temperature increased (figure 5(b)), due to the larger bridge contact angles and thus the reduced ink flow rate. The sheet resistance was the highest at 80 °C and reduced at 100 °C, consistent with line printing observations.

4.2. Doping effect

The section aims to characterize SWCNT lines doped with PEI. In comparison to PEI/SWCNT printing, SWCNT/PEI printing shows consistent resistance.

For SWCNT/PEI lines, the current decreased as the number of PEI deposition layers increased (figure 6(a)) based on *I–V* characterization (inset figure of figure 6(a)). For the repeated tests ($N = 3$), the error bars for the electric current showed ±9.5, ±6.8, ±5.3, ±1.6% for 0, 1, 2, and 3 depositions. With more depositions, the error bars were reduced because semiconducting SWCNTs with various chirality reached current saturation by the doping. Considering the initial p-type SWCNTs, the current decreased due to the PEI' amine group doping. For measurement over 1000 s, the resistance change was only ±0.09%, showing layer stability (figure 6(b)).

For PEI/SWCNT lines, the doping effect was not as reproducible as the SWCNT/PEI lines (figure 6(c)): the SWCNTs might not be fully covered with PEI. The resistance could increase or decrease for forward and backward printing directions (figure 6(d)). The large change in the resistance appeared to be related to the physisorption and reaction with air.

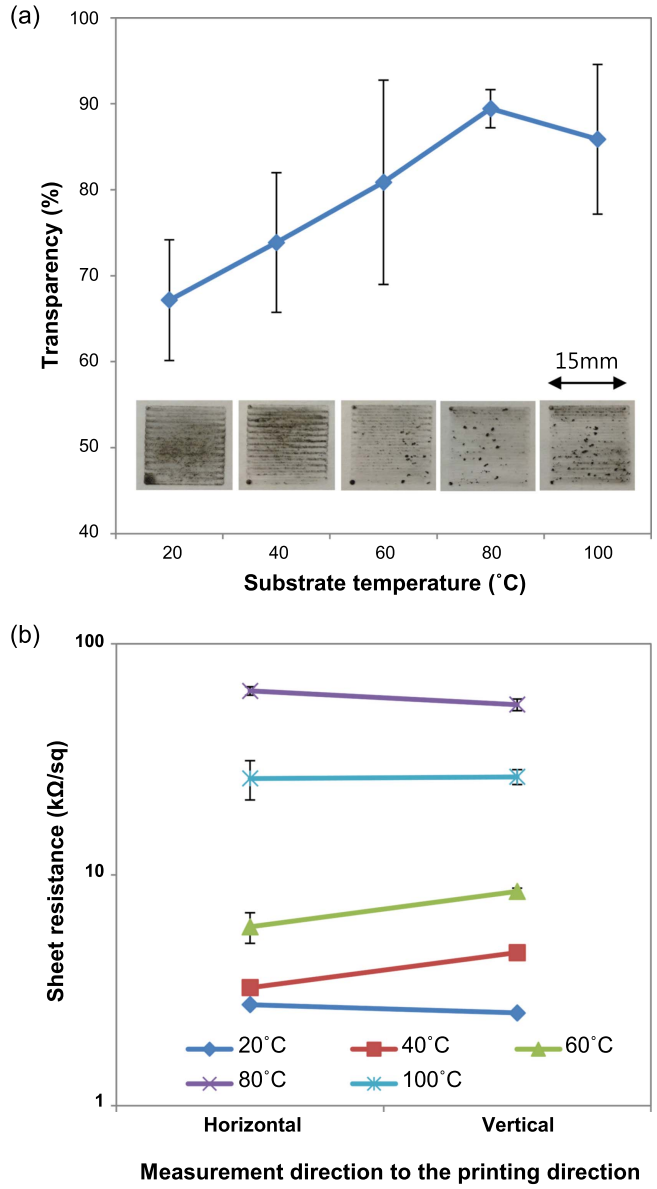


Figure 5. (a) Transparency of printed films at temperatures of 20 °C–100 °C. Printing speed: 1 mm s^{-1} (b) Sheet resistance in the printing and its vertical directions.

When the SWCNT device was placed in a vacuum chamber (125 mmHg), the resistance was constant because of low oxygen environment (figure 6(d)). Figures 6(c) and (d) suggest that the *I*–*V* nonlinearity resulted from the continuous change of PEI/SWCNT resistance due to the interaction with air.

4.3. Sensor evaluation

4.3.1. Gas sensor. The section aims to characterize a SWCNT-gas sensor. When SWCNTs were doped with PEI and Nafion, the sensor showed selectivity due to electrostatic interaction. PEI doped SWCNTs could selectively detect NO_2 while Nafion-doped SWCNTs could selectively detect NH_3.

The non-contact printing technique was used for fabrication of a gas sensor. To achieve uniform resistance, PEI was coated on a SWCNT line. The SWCNT sensor doped with PEI showed a response to NO_2 gas (figure 7(a)). Nafion-doped SWCNTs showed a negligible change when exposed to NO_2 gas but had a significant response to ammonia (supplementary information; figure S9). The specificity of the SWCNT-sensors to NO_2 and ammonia gases were consistent with the previous report [26]. However, the response trends were opposite from the reported trends using n-type SWCNTs. The doping can change the sensitivity and selectivity of a SWCNT sensor [27]. For example, a positively charged dopant makes a SWCNT sensor sensitive to negatively charged gas molecules but insensitive to positively charged gas molecules. Without doping, a SWCNT sensor is also sensitive to gas molecules regardless of the electric charge of gas molecules (supplementary information; figure S9). Note that our results were from the SWCNTs printed on a PET film while the previous report used semiconducting SWCNTs grown on the micromachined electrodes.

4.3.2. pH sensor. The section aims to characterize a SWCNT-pH sensor. The sensitivity showed 61 mV/pH.

For pH measurement, solution drops of pH = 4, 7, and 10 were sequentially interrogated using the fabricated sensor. The potential decreased as pH changed from pH 4 to 10. Note that the actual potential needed to be subtracted from the measured value because a 1.61 V bias potential was added to the circuit. The average slope was 61 mV/pH at 100 s was consistent with the theoretical Nernstian slope. At the low pH between 4 and 7, the sensor showed more stable voltage potential, which agreed with the previous report [28]. In comparison to the previous report, the fabrication method presented in this paper is more cost-effective.

4.4. Discussion

Due to the non-contact nature of the bridge-induced printing, the SWCNTs could be deposited without damaging substrate surface. The contact mode printing with the same capillary pen resulted in scratch marks on the substrate. The print line width was determined by the pen's outside diameter and the contact angle. For the examined ink formulation and substrate type, the contact angle was a function of substrate temperature and print speed. The smallest line width was obtained at $\theta_{B_a} \sim 90°$ and was equal to the outside diameter of a pen nib. According to our characterization, PEI solution with known surface tension coefficient and viscosity showed that the line width was determined by solution viscosity at low speed (supplementary information; figure S8). As the speed increased, the line width was determined by the contact angle and Capillary number. Since the flow rate decreased with the higher contact angle, the resulting sheet resistance increased at the lower flow rate. For example, using the smallest ink drop radius (110 μm) and water surface tension coefficient (0.073 N m), the pressure difference (ΔP) at the substrate surface could range from 0 to 1.3 kPa. At room temperature, ΔP was close to 0 kPa due to the spreading of nanoink, which increased to 1.3 kPa at $\theta_{B_a} = 90°$. Considering that the working principle yields very low pressure gradient

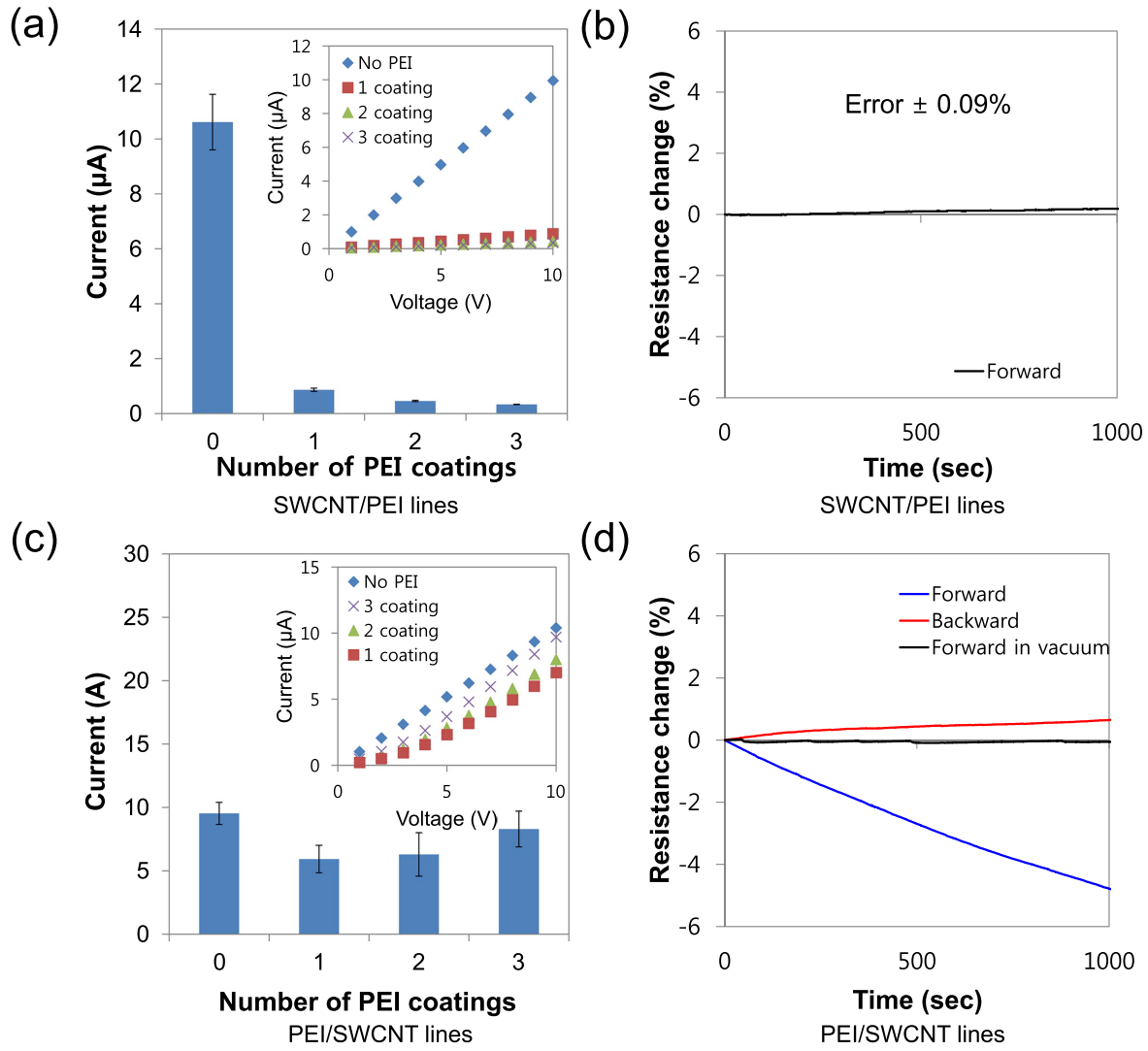


Figure 6. Resistance change for SWCNT/PEI and PEI/SWCNT lines (a) current change at 10 V for 1, 2, and 3-PEI depositions. (b) Resistance change for a SWCNT/PEI line. (c) *I–V* characteristics of PEI/SWCNT lines for 1, 2, and 3-PEI depositions. (d) The resistance change of a SWCNT device for forward and backward printing directions in the air and forward direction in vacuum (125 mmHg).

in the system, the non-contact nanoink bridge-induced printing method can be beneficial for printing water-based molecular ink.

5. Conclusions

In summary, we developed a non-contact capillary pen printing method for fabrication of SWCNT chemical sensors. Using a custom printer, the patterns of a dot, a line, and a film were printed and characterized in the contexts of morphology, electrical properties, and optical transparency. During the printing process, the contact angle was measured and related to the substrate temperatures and printing speeds. For dot printing, a coffee ring effect was clearly shown for a high temperature substrate due to the rapid evaporation and the pinning effect in the ink bridge. The contact angle gradually decreased at room temperature, which formed a relatively uniform height of an SWCNT dot. For line printing, the advancing contact increased as the substrate temperature and the print speed increased. For these conditions, the higher pressure at the substrate reduced the ink flow rate increasing the sheet resistance and the optical transparency of the SWCNT line. For print uniformity, optimal printing temperatures were in the 60 °C–80 °C range. A film could be printed to obtain an average sheet resistance of 7.2 kΩ/sq by a single printing at 60 °C. To obtain consistent high-quality prints, the advancing contact angle needs to be monitored. The nanoink bridge-induced printing allows for printing complex sensor geometries without damage of previous layers. Consistent results have been obtained in the application as a target selective gas sensor and a pH sensor. The non-contact printing approach facilitates printing of large array sensors at low cost for wearable and film-type platforms.

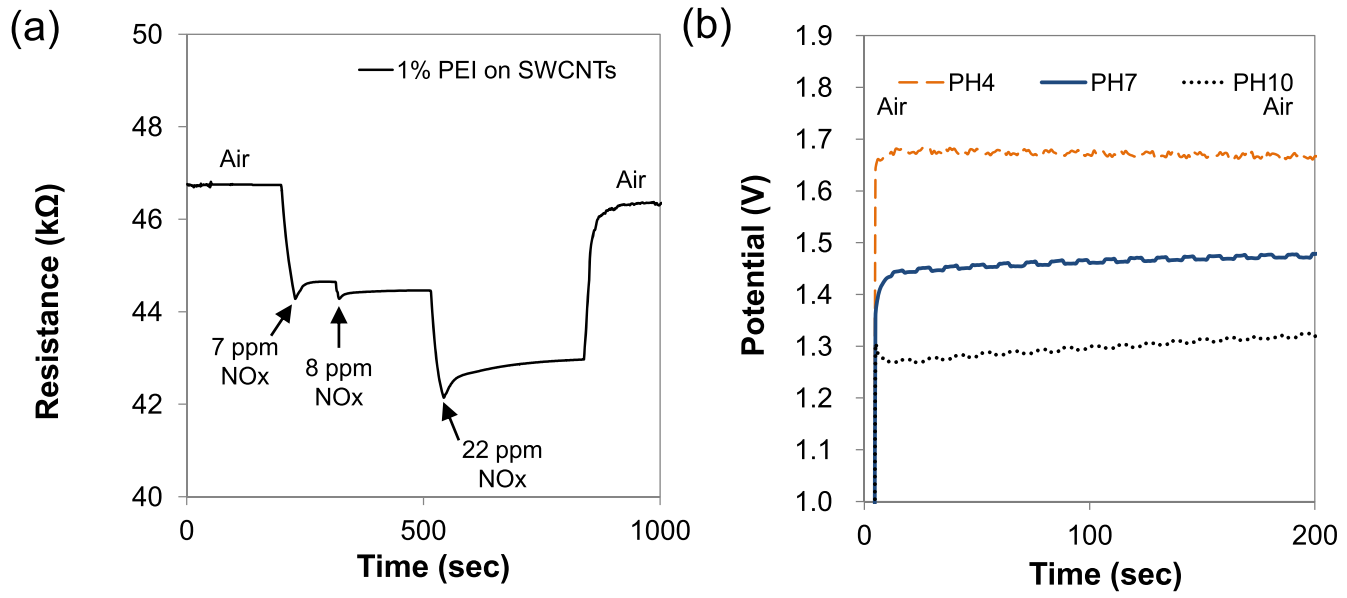


Figure 7. Gas and pH response test (a) change of PEI doped SWCNT resistance for NO_2 gas; PEI is doped on a SWCNT line. (b) The voltage measured for a pH sensor using standard solutions of pH 4, 7, and 10. Note that the voltage is shifted by using a 1.61 V AA battery.

Acknowledgments

SK, BD, JK, and JC acknowledge funding supported from the Office of the Assistant Secretary of Defense for Health Affairs through the Peer Reviewed Medical Research Program under Award No. W81XWH-17-1-0083. Opinions, interpretations, conclusions, and recommendations are those of the author and are not necessarily endorsed by the Department of Defense. IN was partially funded by a grant from the National Institute of Biomedical Imaging and Bioengineering (grant number U01 EB021923).

ORCID iDs

Jae-Hyun Chung https://orcid.org/0000-0002-9861-8559

References

[1] Brown D A, Kim J-H, Lee H-B, Fotouhi G, Lee K-H, Liu W K and Chung J-H 2012 Electric field guided assembly of one-dimensional nanostructures for high performance sensors *Sensors* **12** 5725–51

[2] Burghard M, Duesberg G, Philipp G, Muster J and Roth S 1998 Controlled adsorption of carbon nanotubes on chemically modified electrode arrays *Adv. Mater.* **10** 584–8

[3] Chung J, Lee K H, Lee J and Ruoff R S 2004 Toward large-scale integration of carbon nanotubes *Langmuir* **20** 3011–7

[4] Ko S H, Pan H, Grigoropoulos C P, Luscombe C K, Frechet J M J and Poulikakos D 2007 All-inkjet-printed flexible electronics fabrication on a polymer substrate by low-temperature high-resolution selective laser sintering of metal nanoparticles *Nanotechnology* **18** 345202

[5] Ru C, Luo J, Xie S and Sun Y 2014 A review of non-contact micro- and nano-printing technologies *J. Micromech. Microeng.* **24** 053001

[6] Sirringhaus H, Kawase T, Friend R H, Shimoda T, Inbasekaran M, Wu W and Woo E P 2000 High-resolution inkjet printing of all-polymer transistor circuits *Science* **290** 2123–6

[7] Setti L, Fraleoni-Morgera A, Ballarin B, Filippini A, Frascaro D and Piana C 2005 An amperometric glucose biosensor prototype fabricated by thermal inkjet printing *Biosens. Bioelectron.* **20** 2019–26

[8] Derby B 2010 Inkjet printing of functional and structural materials: fluid property requirements, feature stability, and resolution *Annu. Rev. Mater. Res.* **40** 395–414

[9] Li J, Rossignol F and Macdonald J 2015 Inkjet printing for biosensor fabrication: combining chemistry and technology for advanced manufacturing *Lab Chip* **15** 2538–58

[10] Shimoni A, Azoubel S and Magdassi S 2014 Inkjet printing of flexible high-performance carbon nanotube transparent conductive films by 'coffee ring effect' *Nanoscale* **6** 11084–9

[11] Ta Y L and Yang Z G 2015 Flexible, transparent, thickness-controllable SWCNT/PEDOT:PSS hybrid films based on coffee-ring lithography for functional noncontact sensing device *Langmuir* **31** 13257–64

[12] Tortorich R P and Choi J W 2013 Inkjet printing of carbon nanotubes *Nanomaterials* **3** 453–68

[13] Derby B 2008 Bioprinting: inkjet printing proteins and hybrid cell-containing materials and structures *J. Mater. Chem.* **18** 5717–21

[14] Nishioka G M, Markey A A and Holloway C K 2004 Protein damage in drop-on-demand printers *J. Am. Chem. Soc.* **126** 16320–1

[15] Kim K, Kim G, Lee B R, Ji S, Kim S-Y, An B W, Song M H and Park J-U 2015 High-resolution electrohydrodynamic jet printing of small-molecule organic light-emitting diodes *Nanoscale* **7** 13410–5

[16] Onses M S, Sutanto E, Ferreira P M, Alleyne A G and Rogers J A 2015 Mechanisms, capabilities, and applications of high-resolution electrohydrodynamic jet printing *Small* **11** 4237–66

[17] Park J-U *et al* 2007 High-resolution electrohydrodynamic jet printing *Nat. Mater.* **6** 782–9

[18] Lipomi D J, Vosgueritchian M, Tee B C K, Hellstrom S L, Lee J A, Fox C H and Bao Z N 2011 Skin-like pressure and

strain sensors based on transparent elastic films of carbon nanotubes *Nat. Nanotechnol.* **6** 788–92
[19] Choi T Y, Poulikakos D and Grigoropoulos C P 2004 Fountain-pen-based laser microstructuring with gold nanoparticle inks *Appl. Phys. Lett.* **85** 13–5
[20] Kang B, Min H, Seo U, Lee J, Park N, Cho K and Lee H S 2013 Directly drawn organic transistors by capillary pen: a new facile patterning method using capillary action for soluble organic materials *Adv. Mater.* **25** 4117–22
[21] Schwamb T, Schirmer N C, Burg B R and Poulikakos D 2008 Fountain-pen controlled dielectrophoresis for carbon nanotube-integration in device assembly *Appl. Phys. Lett.* **93** 193104
[22] Han J W, Kim B, Li J and Meyyappan M 2014 A carbon nanotube based ammonia sensor on cellulose paper *RSC Adv* **4** 549–53
[23] Lin C W, Zhao Z B, Kim J and Huang J X 2014 Pencil drawn strain gauges and chemiresistors on paper *Sci. Rep.* **4** 3812
[24] Mirica K A, Azzarelli J M, Weis J G, Schnorr J M and Swager T M 2013 Rapid prototyping of carbon-based chemiresistive gas sensors on paper *Proc. Natl Acad. Sci. USA* **110** E3265–70
[25] Kim J, Moon M-W, Lee K-R, Mahadevan L and Kim H-Y 2011 Hydrodynamics of writing with ink *Phys. Rev. Lett.* **107** 264501
[26] Pengfei Q F, Vermesh O, Grecu M, Javey A, Wang O, Dai H J, Peng S and Cho K J 2003 Toward large arrays of multiplex functionalized carbon nanotube sensors for highly sensitive and selective molecular detection *Nano Lett.* **3** 347–51
[27] Zhang T, Mubeen S, Myung N V and Deshusses M A 2008 Recent progress in carbon nanotube-based gas sensors *Nanotechnology* **19** 33201
[28] Kaempgen M and Roth S 2006 Transparent and flexible carbon nanotube/polyaniline pH sensors *J. Electroanal. Chem.* **586** 72–6